ChemComm

HIGHLIGHT

View Article Online
View Journal | View Issue

Cite this: *Chem. Commun.*, 2025, **61**, 207

Sulfurization of transition metal inorganic electrocatalysts in Li–S batteries

Manchuan Guo,†[a] Zhijie Chen,†[b] Tao Ren,[a] Xiyong Chen[a] and Jinliang Zhu*[a]

Received 14th October 2024,
Accepted 26th November 2024

DOI: 10.1039/d4cc05450d

rsc.li/chemcomm

Lithium–sulfur (Li–S) batteries have garnered significant attention for their exceptional energy density, positioning them as a promising solution for next-generation energy storage. A critical factor in their performance is the use of transition metal inorganic compound electrocatalysts, prized for their distinctive catalytic properties. Recently, increasing interest has focused on the sulfurization of these catalysts in polysulfide-rich environments, a process that holds great potential for enhancing their efficiency. This review analyzes the sulfurization reactions of various transition metal compounds in Li–S batteries and their profound impact on electrochemical performance. By elucidating the sulfurization process with the assistance of advanced characterization techniques, we aim to reveal the true active sites and intrinsic catalytic pathways of sulfur redox electrocatalysts, offering new insights into the design of advanced catalysts for more efficient lithium polysulfide conversion. These findings are expected to accelerate the development of high-performance Li–S battery technologies.

1. Introduction

As the demand for advanced energy storage technologies continues to soar, driven by the rapid growth of new energy transportation and electronic devices,[1,2] lithium–sulfur (Li–S) batteries have emerged as a promising solution. Over the past few decades, Li–S batteries are considered as a promising candidate for next-generation energy storage systems due to their exceptional theoretical energy density ($\approx$2600 W h kg^{-1}), cost-effectiveness, and eco-friendly attributes.[3–6] The electrochemical reactions of Li–S batteries involve a sequential series of solid–liquid–solid transformations.[7] The discharge/charge voltage profile of a typical Li–S battery is illustrated in Fig. 1.[8] The discharge process initiates with a solid–liquid two-phase reaction occurring at approximately 2.4 V (relative to Li/Li$^+$), leading to the transformation of solid sulfur (S_8) into soluble long-chain polysulfides.[9] This is followed by a liquid–liquid reaction, in which long-chain Li_2S_8 is reduced to short-chain Li_2S_6/Li_2S_4. Ultimately, the short-chain polysulfides are converted to solid Li_2S_2/Li_2S with a potential of about 2.1 V. Despite the promising potential of Li–S batteries, their commercialization has been hindered by several key challenges. In particular, the low electrical conductivity of sulfur and lithium sulfides, coupled with the substantial volume changes during cycling, have remained persistent obstacles.[10–14] Furthermore, the internal solid–liquid–solid sulfur transformation process can give rise to the detrimental "shuttle effect", which can lead to rapid capacity fade and impede electrochemical kinetics.[15–19] These issues have collectively posed significant barriers to the development of Li–S batteries, thereby hindering their potential.

To overcome these challenges, various strategies have been developed. One approach is to utilize conductive carbon materials with porous structures as host materials for active substances, which can buffer volume changes while providing a pathway for electron transfer in the electrode.[20–25] Additionally, polar host catalyst materials have been employed to restrict the shuttling of polysulfides. The introduction of polar host electrocatalysts is an effective strategy to address the shuttle effect caused by sulfur redox kinetics in Li–S batteries.[26–29] Transition metal inorganic compound electrocatalysts, such as transition metal nitrides,[30,31] carbides,[32–34] phosphides,[35,36] heterostructures,[37–41] and metal–organic frameworks[42] have been widely proposed to accelerate sulfur conversion and regulate multiphase redox reactions. Great progress has been made in researching the catalysis of polysulfides by transition metal inorganic compound electrocatalysts, but most of them have focused on the redox reactions of polysulfides.[43]

Considering the sulfurization of electrocatalysts in polysulfide-rich environments is essential for gaining a deeper understanding of their behavior and performance in Li–S batteries. Investigating the evolution of these electrocatalysts during charge and discharge cycles is crucial for identifying the

[a] School of Resources, Environment and Materials, Guangxi Key Laboratory of Processing for Non-ferrous Metals and Featured Materials, Guangxi University, Nanning 530004, P. R. China. E-mail: jlzhu@gxu.edu.cn, jlzhu85@163.com
[b] School of Civil and Environmental Engineering, University of New South Wales, Sydney, New South Wales 2052, Australia
† These authors contributed equally to this work.

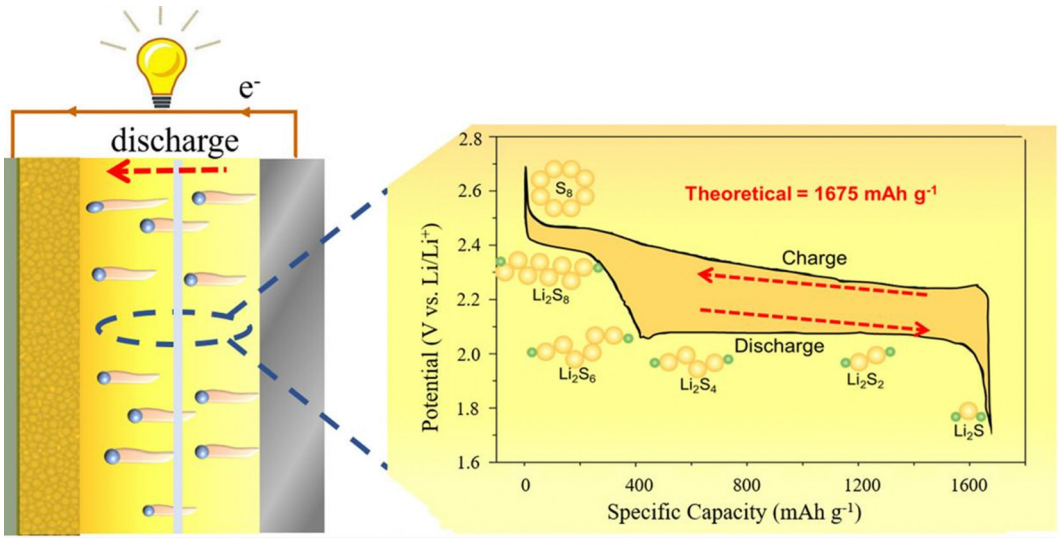

Fig. 1 The diagrammatic sketch and reaction mechanism of Li–S batteries. Reproduced with permission from ref. 8 Copyright (2022) Wiley.

true active sites and intrinsic catalytic mechanisms. Such insights are pivotal for the rational design of high-performance transition metal compound electrocatalysts, which can significantly enhance the efficiency and stability of Li–S batteries. While progress has been made in studying the sulfurization of these electrocatalysts,[44–47] a thorough analysis of their sulfurization chemistry within Li–S batteries remains lacking.

This review provides a comprehensive summary of the research advances on the sulfurization of transition metal inorganic compound electrocatalysts in Li–S batteries, elucidating the sulfurization mechanisms of various electrocatalyst categories, including metal nitrides, metal oxides, metal phosphides, metal sulfides and their heterostructure compounds. Furthermore, we fully analyzed the multiple effects of sulfurization reactions on Li–S battery performance, offering valuable insights for the rational design of high-efficiency electrocatalysts tailored for polysulfide conversion in advanced Li–S batteries.

2. Sulfurization of transition metal inorganic electrocatalysts

In Li–S batteries, the conversion of polysulfides is a complex process involving multiple electrons and significant energy changes. When using transition metal inorganic compound electrocatalysts in Li–S batteries, it is crucial to consider the potential for sulfurization in the polysulfide-rich environment. The interaction between the electrocatalyst and polysulfides may lead to sulfurization, which can affect the catalyst's performance.[48] Therefore, understanding and addressing this process is important to ensure stable catalytic activity during battery operation. Indeed, the electrocatalyst at the solid–liquid interface is susceptible to continuous etching by polysulfides, leading to the formation of defects within the electrocatalyst, which ultimately results in the emergence of new phases. This section analyzed recent achievements on the sulfurization of various transition metal inorganic compounds electrocatalysts, such as nitrides,[49] oxides,[50] and heterostructures.[51,52]

Transition metal nitrides are notable for their exceptional conductivity and adsorption properties, which can be attributed to their capability as conductive Lewis bases due to the presence of lone electron pairs.[53–56] The sulfurization of transition metal nitrides was first investigated in the context of Li–S batteries. In 2018, Qian *et al.*[49] utilized a hydrothermal method to synthesize a range of cobalt-based compounds (Co_4N, CoS_2, Co_3O_4 and CoP) with different anions. Notably, the surface of Co_4N exhibits a notably strong adsorption capacity for Li_2S_6 and Li_2S, with energy values of 9.67 and 7.14 eV respectively, leading to the cleavage of the Li–S bond and subsequent partial sulfurization (Fig. 2(a)). This behavior differs from Co_3O_4, CoS_2, and CoP. However, due to the immaturity of *in situ* characterization techniques at that time, the influence of the sulfide on the redox of polysulfides was not thoroughly examined.

Until 2021, Huang *et al.*[57] conducted a study on the *in situ* electrochemical phase evolution of Co_4N and the effect of the CoS_x substance generated after sulfurization in Li–S batteries. Initially, the low-valent Co in the metal-based precatalyst was subjected to polysulfide etching, resulting in the formation of mosaic block sulfide catalysts (Co–S) during the cycling process, as illustrated in Fig. 2(b). The Co_4N after electrochemical cycling shows superior catalytic polysulfide conversion activity compared to the pristine Co_4N, indicating that the formed CoS_x phase serves as the actual catalytically active site. This catalyst demonstrates high adaptability to polysulfide-rich environments, enhancing polysulfide reaction kinetics at high current rates. High-angle annular dark-field scanning transmission electron microscopy (HAADF-STEM) observations reveal that the resulting mosaic-like catalysts after electrochemical cycling contain both pristine Co_4N phase and various CoS_x phases (Fig. 2(c)). Additionally, thermodynamic computational simulations find that the polysulfide etch-induced phase reconstruction behaviour is universal for all cobalt-based compounds.

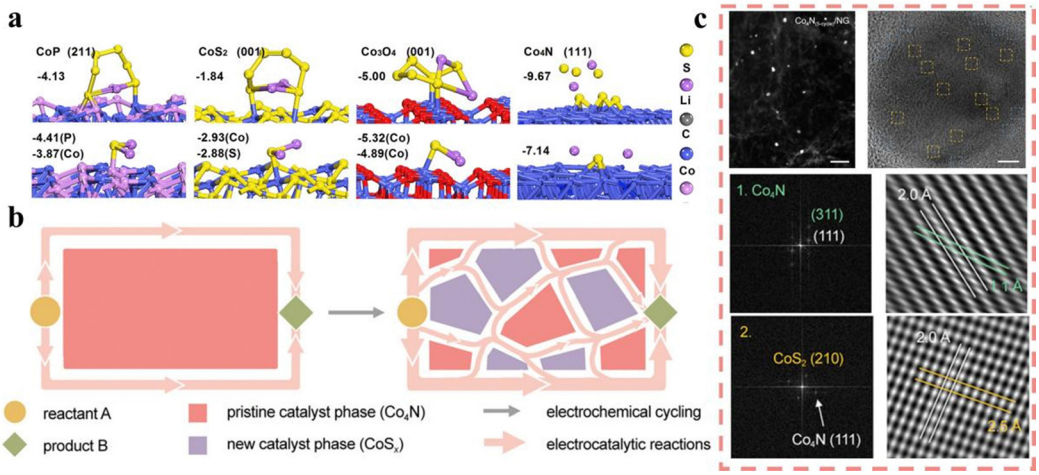

Fig. 2 (a) Adsorption energies of Li_2S_6 and Li_2S on Co-based compounds. Reproduced with permission from ref. 49 Copyright (2018) Elsevier. (b) Representation of Co_4N undergo *in situ* mosaicking phase evolution. (c) HAADF-STEM images, the high-resolution transmission electron microscopy (HRTEM) image and fast Fourier transform (FFT) patterns of $Co_4N_{(5\text{-cycle})}$/NG (nitrogen-doped graphene). Reproduced with permission from ref. 57 Copyright (2020) Wiley-VCH.

These findings represent pioneering efforts in exploring the electrocatalyst evolution, uncovering the dynamic evolution of electrocatalysts during operations. The discovery of CoS_x is characterized by transmission electron microscope (TEM), and no *in situ* characterization technique is used to observe the formation of CoS_x with charging and discharging.

In addition to metal nitrides, metal oxides demonstrate impressive catalytic activity, primarily due to their highly polar surfaces. This strong polarity arises from the oxygen anions in the O^{2-} oxidation state, which enhances their ability to interact with reactants and facilitates catalytic reactions. Therefore, metal oxides are one of the most widely investigated electrocatalysts for Li–S batteries.[58–61] For instance, Peng *et al.*[62] designed a three dimensional (3D) lather-like porous carbon framework containing Fe-based ($Fe_3C/Fe_3O_4/Fe_2O_3$) compounds (named as FeCFeOC), which demonstrates significant chemical reactivity with lithium polysulfide during electrochemical reaction (Fig. 3(a)). They demonstrated that Fe^{3+} in FeCFeOC can react with S_6^{2-} to form

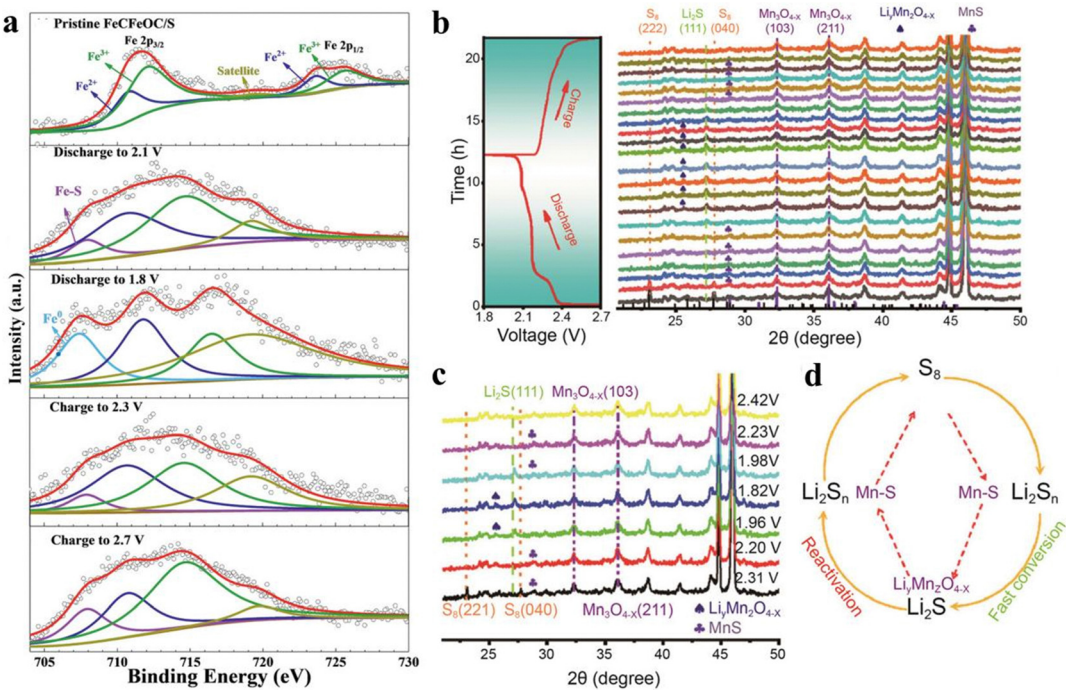

Fig. 3 (a) The Fe 2p XPS spectra of the FeCFeOC/S cathodes. Reproduced with permission from ref. 62 Copyright (2021) Wiley-VCH. (b) *In situ* XRD patterns and the corresponding galvanostatic charge–discharge (GCD) profiles of Mn_3O_{4-x}. (c) Magnified *in situ* XRD patterns. (d) Cycle of sulfur conversion with the Mn_3O_{4-x} catalyst. Reproduced with permission from ref. 50 Copyright (2023) Wiley.

FeS_x species. This was evidenced by comparing the hysteresis loops of FeCFeOC and FeCFeOC–Li_2S_6, where a reduced saturation magnetization was observed in FeCFeOC–Li_2S_6 compared to the original FeCFeOC. Similarly, manganese-based oxides have also been utilized as efficient electrocatalysts in Li–S batteries, Zhang *et al.*[50] developed Mn_3O_{4-x} catalysts with precisely engineered oxygen vacancies to effectively modulate surface charge. *In situ* X-ray diffraction (XRD) patterns confirm that Mn_3O_{4-x} electrocatalysts with oxygen vacancies are transformed to MnS and $Li_yMn_zO_{4-x}$ during discharge (Fig. 3(b)–(d)). MnS generated in the initial discharge stage plays a crucial role in reducing the energetic barriers, thus enhancing the kinetics of the sulfur conversion process. X-ray photoelectron spectroscopy (XPS) and *in situ* XRD techniques were also co-employed to verify the sulfurization of transition metal inorganic compound catalysts, indicating the potential for the application of new techniques to further confirm the sulfurization process.

Besides single-phase transition metal inorganic compounds, sulfurization reactions are also observed for heterostructure catalysts. Zhu *et al.*[52] investigated the sulfurization of VC-VO particles under polysulfide-rich conditions and the effect of vanadium sulfide on the transformation of polysulfides in Li–S batteries. They revealed the sulfide phase evolution of VC-VO particles using *in situ* XRD and Raman techniques during the electrochemical process (Fig. 4(a) and (b)). The results suggest that VC-VO particles containing zero or low-valent metal atoms undergo partial sulfurization, leading to the formation of V_5S_8. This transformation occurs as these particles function as sulfur anode hosts in Li–S batteries. This vanadium sulfide phase exhibits excellent electronic conductivity, accelerating the total electron transfer rate and facilitating the conversion between sulfur species, as supported by density functional theory (DFT) calculations. Furthermore, cyclic voltammetry (CV) tests demonstrate that V_5S_8 primarily affects the transformation of liquid-phase polysulfides. In addition, Zhu *et al.*[51] designed phosphorus-rich MnP, manganese-rich Mn_2P, and MnP–Mn_2P heterostructures with different stoichiometric ratios and investigated their sulfurization processes. They employed *in situ* XRD and *in situ* Raman techniques to reveal the phase transition of MnP–Mn_2P heterostructure particles during the transformation of polysulfides. These heterogeneous particles were partially sulfurized to generate manganese sulfide during the electrochemical reaction. Furthermore, products after the phase change process were further explored by XPS and TEM techniques (Fig. 4(c) and (d)). The mutual coupling between inhomogeneous regions of the heterostructures generates synergistic effects, which anchor and catalytically accelerate polysulfides, achieving the ''adsorption-catalytic'' effect on polysulfides in Li–S batteries. The comprehensive characterization techniques have been successfully used to systematically investigate the occurrence of sulfurization reactions and the formation of metal sulfides (*e.g.*, vanadium sulfide and manganese sulfide).

Furthermore, the formation of metal–sulfur bonds between transition metal inorganic compound electrocatalysts and

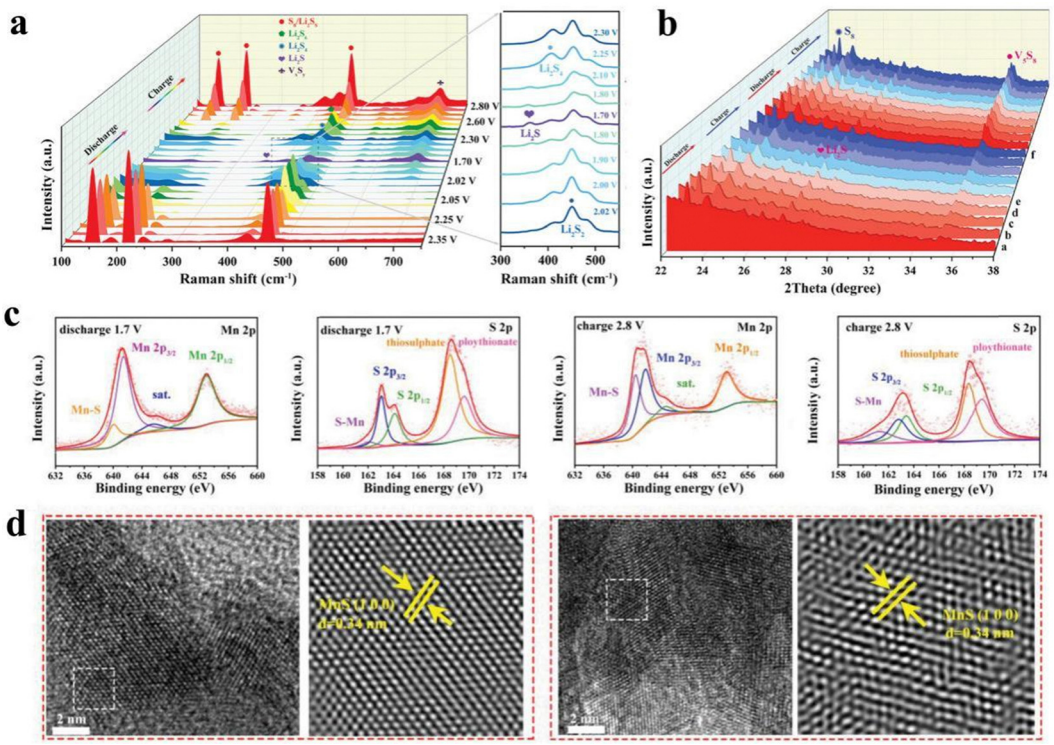

Fig. 4 (a) *In situ* Raman spectra. (b) *In situ* XRD patterns of the VC-VO/HPC@S cathodes. Reproduced with permission from ref. 52 Copyright (2023) Wiley-VCH. (c) Mn 2p, S 2p XPS spectra after discharging to 1.7 V/2.8 V. (d) HRTEM images of MnP–Mn_2P/C@S cathodes after charging to 2.8 V. Reproduced with permission from ref. 51 Copyright (2023) Wiley-VCH.

polysulfides have been investigated.[63] Metal–sulfur bonds can be observed when transition metal inorganic compounds adsorb polysulfide species, although metal sulfide formation may not always occur.[64] However, the sulfurization brings about the formation of metal sulfides. This is the difference between metal–sulfur bonds and sulfurization of transition metal inorganic compound electrocatalysts. Using DFT calculations, researchers have characterized the formation energies and bond lengths of these metal–sulfur bonds.[63,64] Notably, it is imperative to employ *in situ* characterization techniques to ascertain whether sulfurization occurs during electrochemical reactions and to determine whether the metal–sulfur bonds are further sulfurized into metal sulfides.

In situ XRD and *in situ* Raman spectroscopy are indispensable for confirming the formation of sulfurization products. When combined with CV and other electrochemical characterization methods, these techniques enable a comprehensive analysis of the electrochemical behavior of catalysts during Li–S battery operation, offering valuable insights into how sulfurization product formation affects battery performance. Sun *et al.*[65] investigated the sulfurization of defective VSe_2 by designing it using chemical vapor deposition, in order to gain insights into its electrochemical behavior. Interestingly, the *in situ* Raman spectroscopy analysis revealed the presence of VS_2 signals during the electrochemical reactions, with the intensity of the VS_2 signal increasing during discharging and decreasing during charging, indicating a reversible chemical change process (Fig. 5(a)). However, the VS_2 signal of Raman spectroscopy can only demonstrate the bonding of the vanadium with sulfur in the electrocatalyst. More experiments need to be done to verify the generation of VS_2.

Electrochemical CV tests have been employed to investigate the sulfurization of metal fluoride by analyzing the changes in redox peaks. Zhang *et al.*[66] synthesized iron fluoride/graphene (FeF_2@rGO) composites as an electrocatalyst for this purpose. The CV tests were conducted using S-free cells, revealing two prominent reduction peaks in the first cycle. These peaks indicate the conversion of FeF_2 to Li_xFeF_2, followed by its further reduction to LiF and Fe (Fig. 5(b)). Additionally, it is noted that there are no notable redox peaks in the subsequent cycles, suggesting that the phase transition is irreversible during the subsequent charging process. Furthermore, the study delves into the roles of LiF and FeS. It is observed that LiF facilitates efficient ion diffusion for the redox of polysulfides due to its low lithium diffusion barrier, while FeS effectively captured polysulfides through strong polar interactions and accelerated the transformation of polysulfides (Fig. 5(c)).

3. Impacts of sulfurization reactions on lithium–sulfur battery performance

The sulfurization reaction induces the formation of sulfide phases on the original electrocatalyst. The application of

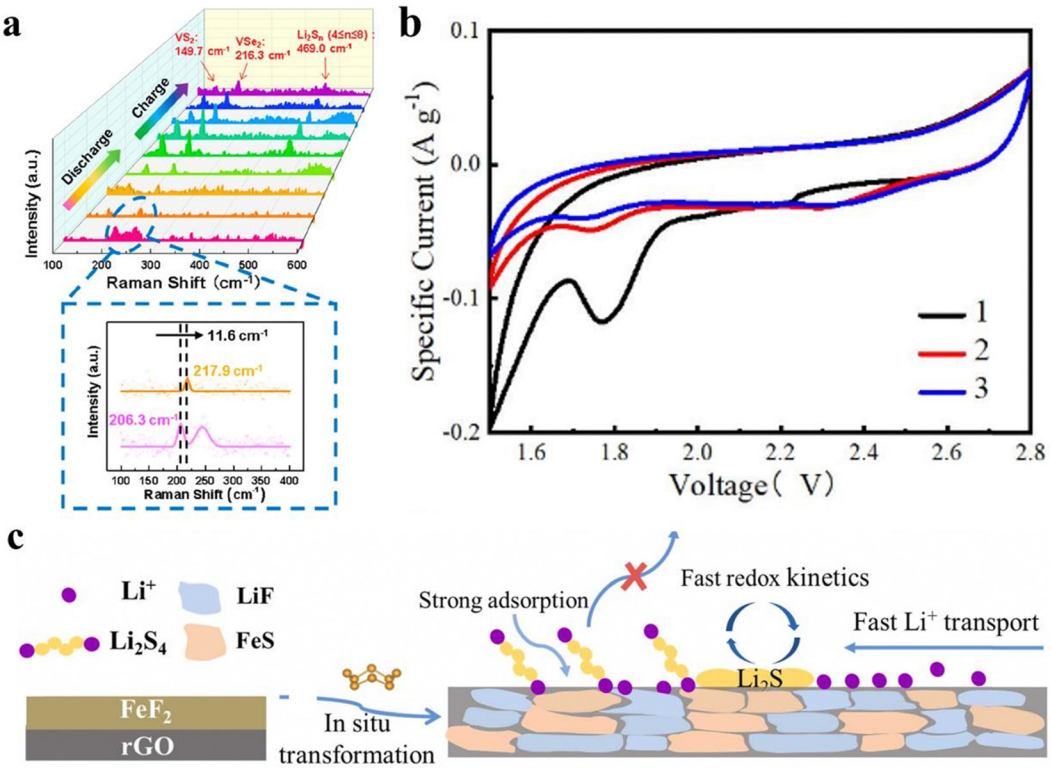

Fig. 5 (a) Operando Raman spectra at different discharge and charge states and the magnified view of the signal of VSe_2. Reproduced with permission from ref. 65 Copyright (2020) American Chemical Society. (b) Cyclic voltammetry curve of FeF_2@rGO cathode without sulfur. (c) Schematic diagram of the cathode catalytic conversion process during the cycle. Reproduced with permission from ref. 66 Copyright (2022) Elsevier.

transition metal sulfides in Li–S batteries have demonstrated that leveraging the polar–polar interactions of sulfides to promote polysulfide conversion through chemical adsorption is highly effective.[67–69] Transition metal sulfides exhibit advantages for electrocatalyst including: (1) a moderate adsorption capacity, which effectively restricts polysulfide shuttling while allowing for unhindered subsequent conversions,[17,70–74] (2) facilitating the reversible transformation of polar lithium sulfide species.[67–69,75,76] For *in situ* sulfurization products (*in situ* generated metal sulfides), They not only exhibit the general advantages of transition metal sulfides but also possess higher polysulfide reactivity, which can be attributed to:

(1) The formation of new active sites on the material surface and interior subsequent to *in situ* sulfurization. Huang *et al.*[57] synthesized bulk Co_4N for application in Li–S batteries, and noted that after cycling, the bulk Co_4N phase underwent sulfurization, resulting in the evolution of the material into an interconnected ensemble of 2–10 nm particles. This *in situ* generated interconnected ultrafine sulfide catalysts possess an abundance of active sites, exhibiting exceptional catalytic performance.

(2) The sulfurization products form heterogeneous interfaces with the original metal compound catalyst. Zhu *et al.*[77] employed heterogeneous MnP–MnO_2 nanoparticles loaded on porous carbon (MnP–MnO_2/C) as a catalyst to enhance the reaction kinetics of lithium polysulfides (LiPSs), and observed that *in situ* sulfurization occurred on the MnP–MnO_2/C, resulting in the formation of MnS on the surface, which led to the creation of a new electrocatalyst with excellent catalytic performance.

Electrode materials after sulfurization can have a dual impact on battery performance (Table 1). The sulfurization process triggers dynamic changes in the local electronic state and structural configuration on the surface of the electrocatalyst, and the presence of sulfide phases can accelerate the kinetic conversion of lithium sulfide, thereby enhancing the overall performance of the battery.

The advantages of *in situ* generated metal sulfide electrocatalysts in Li–S batteries can be summarized as: creating new active sites on the electrocatalyst surface,[57,77,84] improving polysulfide adsorption capability,[67–69] and reducing the polysulfide conversion energy barriers.[78,85–92] These advantages provide important guidance for the design and selection of electrocatalysts in Li–S batteries (Table 2). These principles and corresponding materials suggest that, after *in situ* sulfurization of transition metal compounds as electrocatalysts, new active sites are generally formed, and the sulfurized materials commonly exhibit improved adsorption capacity for polysulfides and reduced energy barriers for polysulfide conversion. Besides, the occurrence of sulfurization and the realization of its benefits require the electrocatalyst to possess certain conditions, and electrocatalysts with the following characteristics are prone to undergo sulfurization and produce favorable outcomes: (1) transition metal compounds materials with defects and vacancies, such as oxygen vacancies,[50] Se vacancies[65,81] or metal ion vacancies.[79] MnV_2O_6 with V defects (D-MVO) exhibits more pronounced *in situ* sulfurization features compared with defect-free MnV_2O_6 (MVO).[79] (2) Compounds containing low-valent transition metal elements.[51,57,83] VC-VO non-uniform particles[52] containing zero-valent or low-valent metal atoms were partially sulfurized to form V_5S_8 in Li–S batteries.

However, the sulfurization reaction may lead to gelation on the electrocatalyst surface, resulting in decreased catalytic activity.[93–96] Some oxides release anionic ligands into the electrolyte, forming sulfates or thiosulfates. This may be attributed to the surface oxidation-reduction reaction between lithium sulfide and transition metal oxides, as well as the over-oxidation of lithium sulfide by LiTFSI in the electrolyte.[78]

3.1 Creating new active sites on the electrocatalyst surface

During the operation of Li–S batteries, the electrocatalyst undergoes a sulfurization reaction in the sulfur-rich working environment, triggering phase transformations on its surface, where transition metal sulfide phases form a coating. This, in turn, alters the active sites of the electrocatalyst, exerting novel influences on the battery's catalytic performance.[57,77,84] Zhu *et al.*[52] developed a novel VC-VO non-uniform particle catalyst

Table 1 Cycling properties of electrode materials exhibiting sulfurization in Li–S batteries

Pristine electrode material/ sulfurization product	Cycle number	Sulfur loading (mg cm^{-2})/content	Electrolyte-to-sulfer ratio (E/S) (μL mg^{-1})	Initial/cycling capacity (mA h g^{-1})	Capacity retention (%)
Mn_3O_4/MnS[50]	1000	1.5/80%	~30	815/553 (1C)	67.85
MnP–Mn_2P/MnS[51]	150	1.8/80%	—	1419/1212 (0.1C)	85.41
VC-VO/V_5S_8[52]	200	1.2/—	—	1484/1309 (0.1C)	88.21
Co_4N/CoS_2[49]	—	~2.1/83.9%	~15	1337/—(0.2C)	—
Co_4N/CoS_x[57]	200	1.0/70%	19	~1100/~726 (4C)	~66.00
FeCFeOC/FeS_x[62]	500	~0.9/70%	~20	963/748 (1.0C)	77.67
VSe_2/VS_2[65]	100	1.4–1.7/—	—	1025/967 (0.5C)	94.34
FeF_2/FeS[66]	100	~1.3/70%	~12	1221/964 (0.2C)	78.95
In_2O_3/$LiInS_2$[78]	500	~1.0/70%	~20	901/721 (0.5C)	80.02
MnV_2O_6/VS_xMnS_x[79]	1000	~1.0/70%	~30	1062.2/465.4 (1C)	43.81
Mo_2C/S–Mo_2C[80]	400	~1.5/80%	—	798/612 (1C)	76.69
$MoSe_2$/MoSeS[81]	400	~/75%	13	1225/980.5 (2C)	80.04
MoS_2/gelated MoS_2[82]	250	1.2/70%	~16	418/— (3C)	—
Cu/Cu_xS[83]	120	~3.2/80%	~15	1432/1196 (0.1C)	83.52
$NiMn_2O_4$/NNMO–MnS_2–Ni_3S_4[84]	100	~1.0/75%	15	1094/952 (0.5C)	87.02
MnP–MnO_2/MnS[77]	200	1.8/75%	20	1511/1299 (0.1C)	85.97

Table 2 Summary table of each principle and corresponding materials

Pristine electrode material	New active site	Suitable adsorption of polysulfides	Reduction of conversion energy barriers	Ref.
Mn_3O_4	MnS	Yes	Yes	50
MnP–Mn_2P	MnS	No	Yes	51
VC-VO	V_5S_8	No	No	52
Co_4N	CoS_2	Yes	No	49
Co_4N	CoS_x	Yes	No	57
FeCFeOC	FeS_x	No	Yes	62
VSe_2	VS_2	No	Yes	65
FeF_2	FeS	Yes	No	66
In_2O_3	$LiInS_2$	Yes	No	78
MnV_2O_6	VS_xMnS_x	Yes	Yes	79
Mo_2C	S–Mo_2C	Yes	Yes	80
$MoSe_2$	MoSeS	No	Yes	81
MoS_2	Gelated MoS_2	No	No	82
Cu	Cu_xS	Yes	No	83
$NiMn_2O_4$	NNMO–MnS_2–Ni_3S_4	Yes	No	84
MnP–MnO_2	MnS	No	No	77

supported on a hierarchical porous carbon (VC-VO/HPC) for application in Li–S batteries. During the electrochemical process, the VC-VO non-uniform particles interact with polysulfides, resulting in the partial decomposition of V_5S_8 on the surface. The generated V_5S_8 acts as a new active catalytic site, accelerating the charge transfer rate, promoting polysulfide conversion, and enhancing battery performance. To further elucidate the role of V_5S_8 in the oxidation-reduction process, electrochemical tests were conducted on cycled VC-VO/$HPC_{(5\text{-cycle})}$ and compared with uncycled VC-VO/HPC and HPC before and after cycling. The CV tests reveal that the oxidation peak of VC-VO/$HPC_{(5\text{-cycle})}$ shifted toward the low-voltage stage, indicating that V_5S_8 significantly suppressed reaction polarization, accelerated the conversion of lithium polysulfide (Fig. 6(a)). Tafel curve analysis shows that V_5S_8 exhibited pronounced catalytic activity, accelerating reaction kinetics (Fig. 6(b)–(d)). Notably, V_5S_8 has a profound accelerating effect on the mutual conversion of soluble polysulfides. This demonstrates that the sulfurization reaction generates new active sites, altering the dynamics of lithium polysulfide conversion.

In a similar vein, the work by Huang *et al.*[57] has elucidated that the low-valent Co in metal-based precatalysts undergoes polysulfide etching, yielding sulfide catalysts (Co–S) during cycling, whEich are the actual active sites. A comparative study of the electrochemical performance of the original CoN catalyst and the catalyst with CoS formed after cycling reveals that the latter exhibits enhanced electrochemical activity in the liquid–liquid polysulfide redox reaction in Li_2S_6 symmetric cells (Fig. 6(e)), characterized by increased response current and enhanced charge transfer. Furthermore, a chronoamperometric investigation on Li_2S_8 batteries (Fig. 6(f)) reveals that CoS accelerates the nucleation and growth of Li_2S.

3.2 Improving polysulfide adsorption capability

In Li–S batteries, the adsorption capacity of the electrocatalyst towards lithium polysulfides plays a pivotal role in determining the smooth progression of the catalytic process. Strategies aimed at enhancing the adsorption capacity of lithium polysulfides *via* polar compounds can effectively promote lithium polysulfide conversion.[67–69] However, in accordance with the Sabatier principle, overly strong adsorption of lithium polysulfides can conversely block the surface reaction sites, thereby hindering the conversion kinetics.[97–102]

Yang *et al.*[78] successfully developed In-based compounds that exhibits stage-specific catalytic effects on lithium polysulfides in Li–S batteries, selectively retarding the dissolution of elemental sulfur into polysulfides and accelerating the deposition of polysulfides into insoluble Li_2S. This tailored catalytic strategy effectively modifies the reaction pathway, and reduces the accumulation of polysulfides in the electrolyte, ultimately suppressing the shuttle effect. Further mechanistic studies reveal that the strong adsorption of sulfur by In-based oxides leads to the formation of a large number of S–In bonds on the surface, thereby slowing down the dissolution of S_8 and generating a probe $LiInS_2$ catalyst (Fig. 7(a)). The XPS spectra of the fully discharged In-based electrode confirm the evolution of $LiInS_2$ (Fig. 7(b) and (c)). Notably, the moderate binding of $LiInS_2$ with lithium polysulfides accelerates the subsequent conversion of lithium polysulfides, underscoring the significance of this selective catalytic approach. Zhang *et al.*[66] found similar phenomena. Following the sulfurization reaction, FeS remains stable in the electrocatalyst, retaining its catalytic activity. Theoretical calculations of its binding energy with Li_2S_4 revealed that FeS exhibits the strongest adsorption capacity compared to LiF and graphene substrates (Fig. 7(d)–(f)), underscoring its role as a powerful anchor site for lithium polysulfides. The assembly of FeF_2@rGO symmetric batteries (Fig. 7(g)) yields higher polarization currents in their CV curves, accompanied by two pairs of sharp oxidation-reduction peaks observed during the scanning process. These results collectively suggest that the FeS component in the cathode can effectively accelerate the reversible conversion of lithium polysulfides, thereby enhancing the overall battery performance.

3.3 Reducing polysulfide conversion energy barriers

The shuttle effect, a pervasive phenomenon in Li–S batteries, poses a significant obstacle to their practical implementation.[15–19] Specifically, when the concentration of dissolved lithium polysulfides in the electrolyte reaches a critical threshold, they tend to

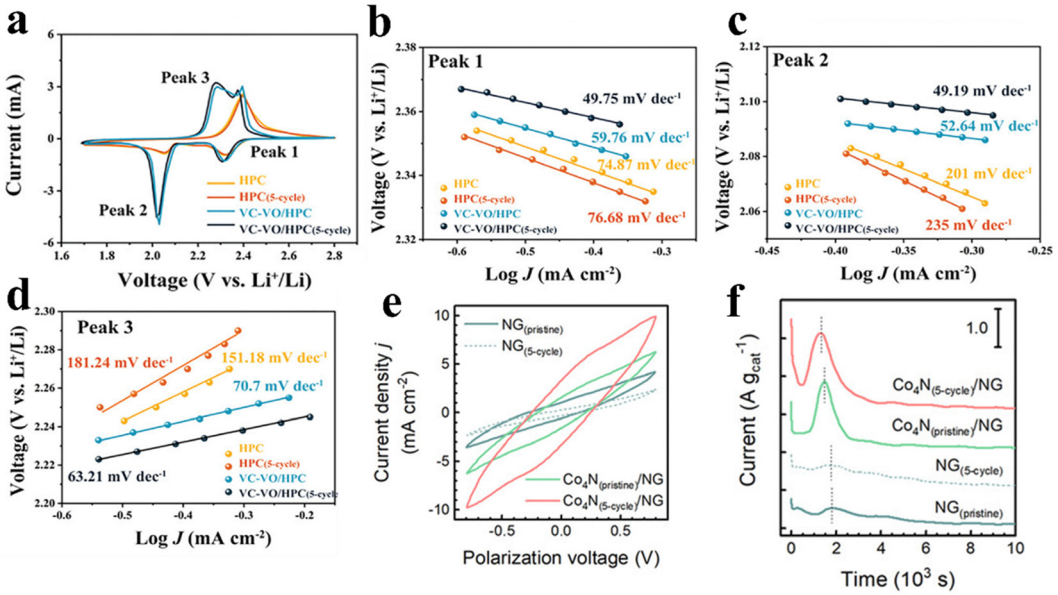

Fig. 6 The effect of electrochemical phase evolution on catalytic performance toward various polysulfide-involving reactions. (a) CV profiles of VC-VO/$HPC_{(5\text{-cycle})}$, VC-VO/HPC, $HPC_{(5\text{-cycle})}$, and HPC at a scan rate of 0.1 mV s^{-1}. Tafel plots of (b) peak 1, (c) peak 2, and (d) peak 3. Reproduced with permission from ref. 52 Copyright (2023) Wiley-VCH. Four types of electrode, $NG_{(pristine)}$ (nitrogen-doped graphene), $NG_{(5\text{-cycle})}$, $Co_4N_{(pristine)}$/NG, and $Co_4N_{(5\text{-cycle})}$/NG, served as working electrodes. (e) CV curves of $Li_2S_6|Li_2S_6$ symmetric cells, showing the kinetics of liquid–liquid polysulfide interconversion. (f) Chronoamperometry curves of $Li|Li_2S_8$ cells, showing the kinetics of liquid–solid Li_2S deposition. Reproduced with permission from ref. 57 Copyright (2020) Wiley-VCH.

migrate to the negative electrode, causing a loss of active materials and passivation of the lithium anode. This process ultimately leads to rapid capacity decay and, in severe cases, catastrophic failure of the battery. A promising strategy to mitigate the shuttle effect involves the design and utilization of electrocatalysts with enhanced catalytic activity,[49,78,85–92] which can accelerate the conversion of intermediate products and thereby suppress the detrimental effects of polysulfide shuttling (Fig. 8(a)).

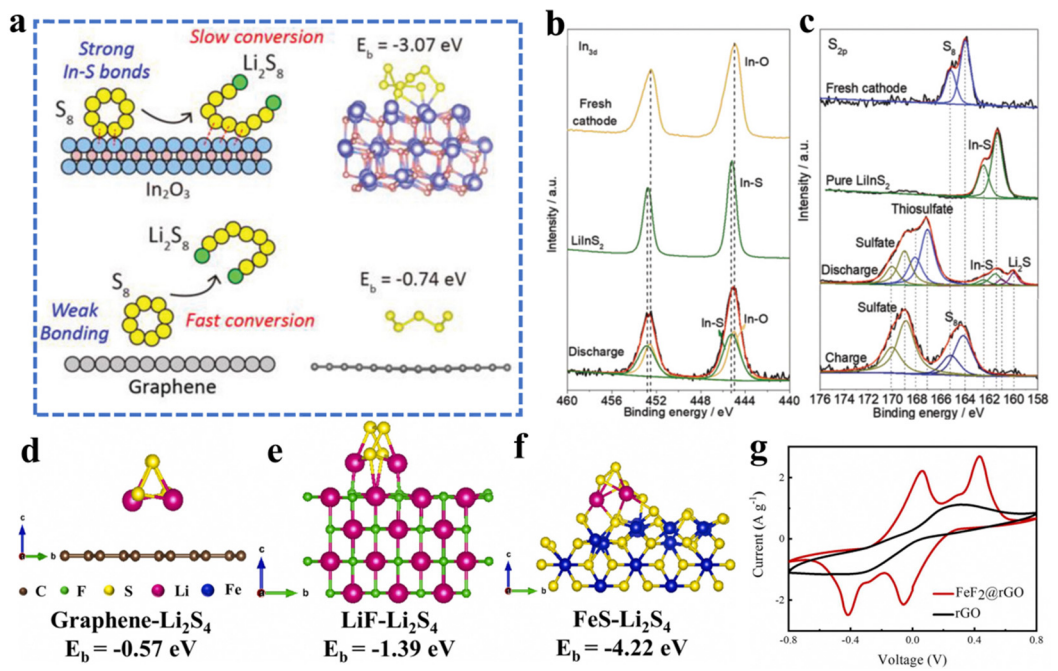

Fig. 7 (a) Binding energy of −3.07 eV between In_2O_3 and S_8. (b) XPS spectra for the 3d level of In in pristine In_2O_3, prepared $LiInS_2$ and the In-based cathode in the fully discharged state; (c) S_{2p} XPS spectra of fresh cathode, pure $LiInS_2$ and the In-based cathode in the fully discharged and charged state; reproduced with permission from ref. 78 Copyright (2021) Wiley-VCH. Atomic configuration and corresponding binding energy after adsorption of Li_2S_4, (d) rGO, (e) LiF and (f) FeS. (g) CV curves of FeF_2 @rGO and rGO symmetric batteries. Reproduced with permission from ref. 66 Copyright (2022) Elsevier.

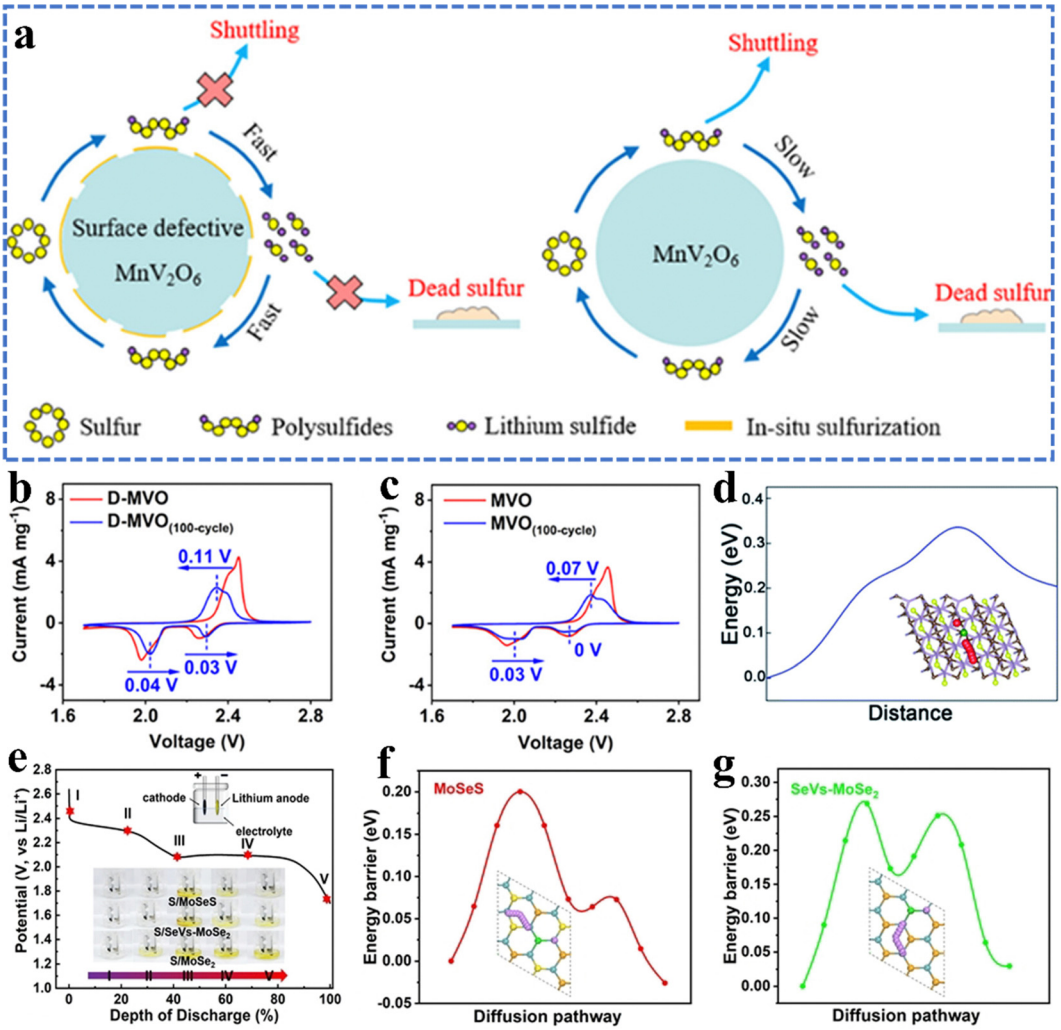

Fig. 8 (a) Schematic illustration of accelerating lithium polysulfide conversion to suppress shuttle effect and prevent dead lithium accumulation. CV curves with (b) D-MVO and (c) MVO separators of the 1st and 100th cycle. Reproduced with permission from ref. 79 Copyright (2022) American Chemical Society. (d) Reaction profile of Li_2S decomposition on S–Mo_2C (101). The inset shows the reaction pathway. The black, light purple, yellow, green, and red balls represent C, Mo, and S bonded with Mo, S of LiPSs, and Li, respectively. Reproduced with permission from ref. 80 Copyright (2020) Royal Society of Chemistry. (e) *In situ* observation of the transparent electrolyte in Li–S cells with different electrocatalysts. Dissociation energy barrier profiles from Li_2S to (Li + LiS) on (f) MoSeS and (g) SeVs–$MoSe_2$. (Inset: The dissociation pathway.) Reproduced with permission from ref. 81 Copyright (2021) Wiley-VCH.

To accelerate lithium polysulfide conversion, Zhang *et al.*[79] successfully developed defective MnV_2O_6 (D-MVO) as a pre-catalyst for LiPSs adsorption and conversion. During the electrochemical cycling process, the rich defects in D-MVO undergo *in situ* sulfurization, transforming into a highly active catalyst that significantly enhances its catalytic activity towards lithium polysulfides. In contrast, they also prepared defect-free MnV_2O_6 (MVO) and found that the sulfurization ratio of MVO was substantially lower. To elucidate the catalytic activity before and after sulfurization, they compared the CV curves of Li–S batteries using MVO and D-MVO separators for the 1st and 100th cycles. Notably, the overpotential of the battery decreases from 472 mV in the 1st cycle to 323 mV in the 100th cycle when using the D-MVO separator (Fig. 8(b)), unequivocally demonstrating that *in situ* sulfurization enhances the electrocatalytic conversion ability of LiPSs. In stark contrast, the battery using the MVO separator only exhibits a slight shift in the oxidation-reduction peaks after 100 cycles (Fig. 8(c)). This stark difference underscores the significance of *in situ* sulfurization in generating a highly active electrocatalyst that facilitates efficient lithium polysulfide conversion.

To gain deeper insights into the mechanism of sulfurization-enhanced electrocatalysts in promoting lithium polysulfide cycling conversion, Feng *et al.*[80] performed a comprehensive investigation on the sulfurized S–Mo_2C (101) surface, demonstrating its exceptional ability to promote lithium polysulfide conversion. To elucidate the underlying mechanism, they employed the climbing image nudged elastic band method to calculate the decomposition energy barrier. The results show that the dissociation energy of Li_2S on S–Mo_2C (101) is approximately 0.20 eV, with an estimated decomposition barrier of 0.38 eV, as illustrated in Fig. 8(d). Notably, this barrier is remarkably

low, comparable to that of the optimal VS_2 anchor material (0.31 eV), indicating that a significantly lower overpotential is required for the initial charging process. The findings collectively suggest that the sulfurized Mo_2C (101) surface successfully integrates the advantages of strong LiPSs binding, low reduction barriers, and low decomposition barriers, ultimately leading to exceptional electrochemical performance.

Similarly, Sun *et al.*[81] investigated the electrocatalytic behavior of the $MoSe_2$ precursor before and after *in situ* sulfurization. They synthesized a Se-vacancy-containing $MoSe_2$ precursor, which was sulfurized to form MoSeS during the lithium–sulfur battery cycling process. Notably, MoSeS acts as a true catalyst to promote the conversion of lithium polysulfides. As the discharge continued, MoSeS undergoes further sulfurization to form MoS_x/$MoSe_x$. After the charging process, MoS_x/$MoSe_x$ gradually disappeared, and MoSeS is regenerated to participate in the next cycle. To elucidate the catalytic activity of the electrocatalysts, they assembled transparent batteries with SeVs–$MoSe_2$, MoSeS, or bare $MoSe_2$ loaded on carbon cloth to monitor the instantaneous changes in LiPSs. When the three batteries are discharged to 2.35 V, no obvious color changes are observed (Fig. 8(e)). When discharged to the second plateau (2.10 V), the electrolyte turned bright yellow. After discharge, the yellow color faded slightly due to the formation of insoluble Li_2S_2 and Li_2S. It was evident that a pale yellow color was observed at the end of discharge for MoSeS and SeVs–$MoSe_2$, whereas no obvious color change was observed for the bare $MoSe_2$ battery, indicating that the conversion of LiPSs was facilitated. To gain deeper insights into the reason for the enhanced LiPSs conversion on defective electrocatalysts, they also simulated the distribution and pathways of Li_2S dissociation energy barriers (Fig. 8(f) and (g)). The corresponding dissociation barriers decrease from 1.08 eV for bare $MoSe_2$ to 0.27 eV for SeVs–$MoSe_2$ and 0.20 eV for MoSeS, indicating that the new electrocatalyst formed after sulfurization accelerates the kinetic reaction of Li_2S dissociation. This result unequivocally demonstrates that the actual catalyst MoSeS promotes the conversion of lithium polysulfides by reducing the reaction energy barriers and facilitates the dissociation of Li_2S, achieving bidirectional sulfur conversion and further enhancing the redox kinetics in Li–S chemistry.

3.4 Risks of active material loss and surface gelation after sulfurization reconstruction of catalysts in Li–S batteries

The sulfurization reconstruction of electrocatalysts in Li–S batteries primarily involves the reaction between the catalyst and elemental sulfur or lithium sulfide,[49,57,79–81] which inevitably leads to the consumption of active materials within the battery. However, there is still a lack of research on the quantitative assessment of active material consumption following sulfurization. Recently, the surface gelation of electrochemical catalysts has also been observed and studied, but further investigation is needed to fully understand its impact on catalyst performance and longevity.[103,104] However, unlike sulfurization reconstruction, surface gelation leads to a weakening of the catalytic activity of the catalyst towards polysulfides, and the capacity of the lithium–sulfur battery decreases after gelation.[93–96] This phenomenon highlights the risks of designing suitable electrochemical catalysts through sulfurization reconstruction.

Notably, Zhang's team[82] was the first to discover the surface gelation of electrochemical catalysts (MoS_2, FeS_2, CoS_2, NiS_2, and WS_2) in Li–S batteries. From a microscopic mechanism perspective, the positively charged Mo atoms in MoS_2, which are Lewis acid sites, interact with 1, 3-dioxolane (DOL) in the lithium–sulfur battery electrolyte, causing DOL to undergo ring-opening polymerization and form a gel. The resulting gel layer is amorphous, with a smooth surface, and adheres to the surface of the MoS_2 catalyst, resulting in a decrease in catalytic activity. They selected MoS_2 as the material for their experimental investigation, The detrimental effect of gelation on the electrochemical activity of MoS_2 can be clearly observed

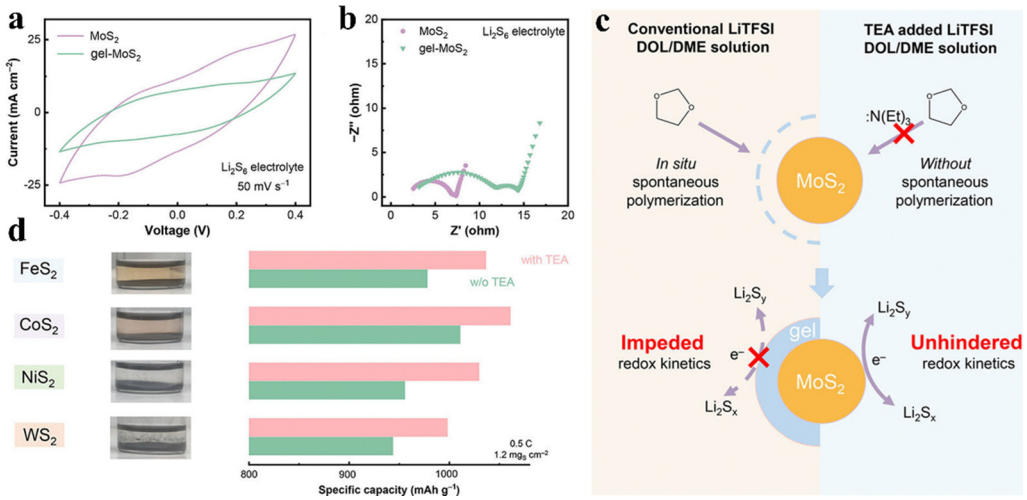

Fig. 9 (a) Schematic of the surface-gelation and gelation-inhibition processes in Li–S batteries with conventional or TEA solution. Surface gelation effect on MoS_2 in sulfur redox electrocatalytic performances. MoS_2 separators and gel–MoS_2 separators were adopted in the cells. (b) CV profiles and (c) EIS profiles of Li_2S_6 symmetric cells. (d) Gelation-inhibition using TEA on FeS_2, CoS_2, NiS_2, and WS_2 electrocatalysts (left) and corresponding comparison on specific capacity after 40 cycles in Li–S cells (right). Reproduced with permission.[82] Copyright 2021, Wiley-VCH.

through CV and electrochemical impedance spectroscopy (EIS) tests of the Li_2S_6 symmetric cell. Fig. 9(a) and (b) illustrate that the peak current response of the symmetric cell assembled with gelated MoS_2 is substantially lower than that of the original ungelated MoS_2, indicating a significant impairment of its electrochemical activity. Moreover, the EIS evaluation reveals a passivation tendency of the surface gel layer, further corroborating the deleterious impact of gelation on the electrochemical performance of MoS_2.

To mitigate the gelation issue, Zhang's team employed triethylamine (TEA) as a competitive inhibitor to suppress the surface gelation reaction, as illustrated in Fig. 9(c). This approach successfully prevents the formation of gel on the catalyst surface and is also effective for a range of transition metal disulfides, including FeS_2, CoS_2, NiS_2, and WS_2. When 1.0 vol% TEA was added, no gelation was observed on the surface of these disulfides, and the capacity was significantly enhanced. This indicates that in the absence of gelation, the surface of the disulfides exposes more active sites, thereby facilitating electrocatalytic activity. The investigation into the gelation phenomenon in Li–S batteries serves as a reminder of the importance of delving deeper into the *in situ* reconstruction phenomenon to gain a better understanding of the behavior of catalysts in these batteries. The sulfurization process, which forms sulfides as new catalytic sites that participate in the reaction, raises questions about whether this process will lead to a decrease in active materials and the risk of gelation, and further research is needed to explore these issues.

4. Conclusions and outlook

In Conclusion, the sulfurization reactions of transition metal catalysts (*e.g.*, nitrides, oxides, selenides, sulfides, and heterostructures) with polysulfides in Li–S batteries play a critical role in addressing the shuttle effect, a major hurdle to the commercialization of Li–S batteries. Thorough investigation into the sulfurization mechanism, alongside advanced *in situ* characterization techniques, is crucial for revealing the real active centers and improving the catalytic activity of electrocatalysts. This deeper understanding of the sulfurization process will not only enhance the performance and stability of Li–S batteries but also provide critical insights into the relationship between sulfurization and the electrochemical properties of the system. The findings discussed in this review aim to serve as a foundation for future research, guiding the design of more efficient and stable electrocatalysts while advancing the commercialization of Li–S batteries.

Honestly, research on *in situ* sulfurization of transition metal compounds has yielded significant breakthroughs. The sulfurization process generates transition metal sulfides on the original electrocatalyst surface, creating new active sites that participate in subsequent polysulfide conversions, thereby enriching the electrocatalyst's active site. These newly formed sites exhibit excellent affinity for polysulfides, effectively anchoring them and mitigating the shuttle effect. Moreover, the *in situ* generated transition metal sulfides can lower the reaction energy barrier for polysulfide conversion, thereby accelerating the polysulfide reaction kinetics.

Although research has been conducted on the sulfurization process of transition metal inorganic compound electrocatalysts, there remain challenges in integrating its mechanism with surface-controllable sulfurization for precise catalytic regulation. Furthermore, in the design of electrocatalysts, the risks of active species reduction and surface agglomeration during the *in situ* sulfurization process should also be taken into consideration. To overcome these challenges, several aspects require focused attention. First, a deeper exploration of the relationship between the chemical composition, distribution, and catalytic activity of each component in catalysts after sulfurization is necessary. Comparative experiments must be performed to elucidate the specific effects of each component on polysulfide conversion, as current catalytic mechanisms are largely based on theoretical models. Second, the development and application of advanced characterization techniques, particularly *in situ* methods such as XRD, Raman spectroscopy, X-ray absorption spectroscopy, and small-angle neutron scattering, combined with first-principles computational and thermodynamic simulations, are critical for probing electrocatalyst sulfurization in real time. Moreover, understanding how varying degrees of sulfurization influence polysulfide conversion will help identify the true active centers of these catalysts, providing key insights for optimizing their catalytic activity and stability.

Data availability

No primary research results, software or code have been included and no new data were generated or analysed as part of this invited review.

Conflicts of interest

The authors declare no conflict of interest.

Acknowledgements

This work was supported by the National Natural Science Foundation of China (52462027), and Natural Science Foundation of Guangxi (2022GXNSFAA035463).

Notes and references

1 F. Wu, J. Maier and Y. Yu, *Chem. Soc. Rev.*, 2020, **49**, 1569–1614.
2 Z. P. Cano, D. Banham, S. Ye, A. Hintennach, J. Lu, M. Fowler and Z. Chen, *Nat. Energy*, 2018, **3**, 279–289.
3 G. Zhou, H. Chen and Y. Cui, *Nat. Energy*, 2022, **7**, 312–319.
4 P. G. Bruce, S. A. Freunberger, L. J. Hardwick and J.-M. Tarascon, *Nat. Mater.*, 2012, **11**, 19–29.
5 A. Manthiram, Y. Fu, S.-H. Chung, C. Zu and Y.-S. Su, *Chem. Rev.*, 2014, **114**, 11751–11787.
6 A. Manthiram, S.-H. Chung and C. Zu, *Adv. Mater.*, 2015, **27**, 1980–2006.
7 S. Liu, J. Luo, Y. Xiong, Z. Chen, K. Zhang, G. Rui, L. Wang, G. Hu, J. Jiang and T. Mei, *Front. Chem.*, 2021, **9**, 638557.

8 R. Deng, M. Wang, H. Yu, S. Luo, J. Li, F. Chu, B. Liu and F. Wu, *Energy Environ. Mater.*, 2022, **5**, 777–799.
9 G. Li, S. Wang, Y. Zhang, M. Li, Z. Chen and J. Lu, *Adv. Mater.*, 2018, **30**, 1705590.
10 S. Lang, S.-H. Yu, X. Feng, M. R. Krumov and H. D. Abruña, *Nat. Commun.*, 2022, **13**, 4811.
11 M. Zhao, B.-Q. Li, H.-J. Peng, H. Yuan, J.-Y. Wei and J.-Q. Huang, *Angew. Chem., Int. Ed.*, 2020, **59**, 12636–12652.
12 J. He and A. Manthiram, *Energy Storage Mater.*, 2019, **20**, 55–70.
13 M. Wang, Y. Song, Z. Sun, Y. Shao, C. Wei, Z. Xia, Z. Tian, Z. Liu and J. Sun, *ACS Nano*, 2019, **13**, 13235–13243.
14 X. Wang, Y. Yang, C. Lai, R. Li, H. Xu, D. H. S. Tan, K. Zhang, W. Yu, O. Fjeldberg, M. Lin, W. Tang, Y. S. Meng and K. P. Loh, *Angew. Chem., Int. Ed.*, 2021, **60**, 11359–11369.
15 S. Nanda, A. Bhargav, Z. Jiang, X. Zhao, Y. Liu and A. Manthiram, *Energy Environ. Sci.*, 2021, **14**, 5423–5432.
16 Y.-Q. Peng, M. Zhao, Z.-X. Chen, Q. Cheng, Y. Liu, X.-Y. Li, Y.-W. Song, B.-Q. Li and J.-Q. Huang, *Nano Res.*, 2023, **16**, 8253–8259.
17 Z. W. Seh, J. H. Yu, W. Li, P.-C. Hsu, H. Wang, Y. Sun, H. Yao, Q. Zhang and Y. Cui, *Nat. Commun.*, 2014, **5**, 5017.
18 S.-H. Chung and A. Manthiram, *Joule*, 2018, **2**, 710–724.
19 Y. Pan, Y. Zhou, Q. Zhao, Y. Dou, S. Chou, F. Cheng, J. Chen, H. K. Liu, L. Jiang and S. X. Dou, *Nano Energy*, 2017, **33**, 205–212.
20 D. Fang, Y. Wang, C. Qian, X. Liu, X. Wang, S. Chen and S. Zhang, *Adv. Funct. Mater.*, 2019, **29**, 1900875.
21 H. Ye, J. Sun, S. Zhang, H. Lin, T. Zhang, Q. Yao and J. Y. Lee, *ACS Nano*, 2019, **13**, 14208–14216.
22 H. Zhang, L. Yang, P. Zhang, C. Lu, D. Sha, B. Yan, W. He, M. Zhou, W. Zhang, L. Pan and Z. Sun, *Adv. Mater.*, 2021, **33**, 2008447.
23 X. Ji, K. T. Lee and L. F. Nazar, *Nat. Mater.*, 2009, **8**, 500–506.
24 Z. Wu, Y. Zhang, P. Takyi-Aninakwa, Y. Hu, Z. Lu and Y. Song, *Chem. Commun.*, 2024, **60**, 11108–11111.
25 Y. Wang, Y. Wang, C. Huang, Q. Zhang, Z. Liu and F. Zhang, *Chem. Commun.*, 2023, **59**, 13458–13461.
26 K. Zhang, L. Wu, Z. Xu, C. Zhang, Q. Yang, W. Qian, G. Hu, W. Hu, Y. Kong, J. Zhang, L. Wang and G. Li, *J. Alloys Compd.*, 2023, **947**, 169637.
27 J. Xiao, H. Wei, X. Sun, T. Yang, X. Wu, Y. Song and C. He, *Chem. Commun.*, 2024, **60**, 3962–3965.
28 D.-G. Wang, Y. Wang, M. Song, G.-C. Kuang and K. Han, *Chem. Commun.*, 2019, **55**, 13247–13250.
29 Y. Tian, H. Huang, G. Liu, R. Bi and L. Zhang, *Chem. Commun.*, 2019, **55**, 3243–3246.
30 L. Zhang, X. Chen, F. Wan, Z. Niu, Y. Wang, Q. Zhang and J. Chen, *ACS Nano*, 2018, **12**, 9578–9586.
31 G. H. Park, W.-G. Lim, Y. H. Jeong, S. K. Kang, M. Kim, J. Ji, J. Ha, S. R. Mangishetti, S. Kim, Y. Park, C. Jo and W. B. Kim, *Small Struct.*, 2024, 2400293.
32 B. Wei, C. Shang, X. Wang and G. Zhou, *Chem. Commun.*, 2020, **56**, 14295–14298.
33 X. Zhang, Y. Chen, D. Cai, C. Zhang, Q. Chen and H. Zhan, *Chem. Eng. J.*, 2024, **498**, 155028.
34 H.-J. Xiong, Y.-L. Luo, D.-R. Deng, C.-W. Zhu, J.-X. Song, J.-C. Weng, X.-H. Fan, G.-F. Li, Y. Zeng, Y. Li and Q.-H. Wu, *J. Colloid Interface Sci.*, 2024, **668**, 448–458.
35 S. Yu, W. Cai, L. Chen, L. Song and Y. Song, *J. Energy Chem.*, 2021, **55**, 533–548.
36 P. Feng, Q. Wu, Y. Rodriguez Ayllon and Y. Lu, *Chem. – Eur. J.*, 2024, **30**, e202401345.
37 J. Zhu, X. Dong, Q. Zeng, F. Liang, S. Ning, G. Wang, P. K. Shen and S. Ma, *Chem. Eng. J.*, 2023, **460**, 141811.
38 H.-E. Wang, K. Yin, X. Zhao, N. Qin, Y. Li, Z. Deng, L. Zheng, B.-L. Su and Z. Lu, *Chem. Commun.*, 2018, **54**, 12250–12253.
39 J. Lee, S. Kim, J. B. Park, D. Park, S. Lee, C. Choi, H. Lee, G. Jang, Y. S. Park, J. Yun, S. Moon, S. Lee, C.-S. Jeong, J. H. Kim, H.-J. Choi, D.-W. Kim and J. Moon, *Small*, 2024, **20**, 2406018.
40 Y. Cui, S. Ji, Y. Zhu and J. Xi, *J. Colloid Interface Sci.*, 2024, **675**, 1119–1129.
41 V. P. Nguyen, Y. Qureshi, H. C. Shim, J. M. Yuk, J.-H. Kim and S.-M. Lee, *Small Struct.*, 2024, **5**, 2400196.
42 W. Li, X. Guo, P. Geng, M. Du, Q. Jing, X. Chen, G. Zhang, H. Li, Q. Xu, P. Braunstein and H. Pang, *Adv. Mater.*, 2021, **33**, 2105163.
43 C. Zhang, Y. Ma, X. Zhang, S. Abdolhosseinzadeh, H. Sheng, W. Lan, A. Pakdel, J. Heier and F. Nüesch, *Energy Environ. Mater.*, 2020, **3**, 29–55.
44 J. Xiang, W. Shen, Z. Guo, J. Meng, L. Yuan, Y. Zhang, Z. Cheng, Y. Shen, X. Lu and Y. Huang, *Angew. Chem., Int. Ed.*, 2021, **60**, 14313–14318.
45 J. Wu, T. Ye, Y. Wang, P. Yang, Q. Wang, W. Kuang, X. Chen, G. Duan, L. Yu, Z. Jin, J. Qin and Y. Lei, *ACS Nano*, 2022, **16**, 15734–15759.
46 Q. Liu, C. Zhang, M. Ren, J. Wang, L. Feng, Y. Wang, C. Liu, N. Xiao and H. Zhang, *Colloids Surf., A*, 2024, **692**, 134055.
47 B. Ma, Z. Yang, Z. Yuan and Y. Chen, *Int. J. Hydrogen Energy*, 2019, **44**, 1620–1626.
48 M. Zhao, H.-J. Peng, Z.-W. Zhang, B.-Q. Li, X. Chen, J. Xie, X. Chen, J.-Y. Wei, Q. Zhang and J.-Q. Huang, *Angew. Chem., Int. Ed.*, 2019, **58**, 3779–3783.
49 J. Zhou, X. Liu, L. Zhu, J. Zhou, Y. Guan, L. Chen, S. Niu, J. Cai, D. Sun, Y. Zhu, J. Du, G. Wang and Y. Qian, *Joule*, 2018, **2**, 2681–2693.
50 Y. Zhu, Y. Zuo, X. Jiao, R. Manjunatha, E. R. Ezeigwe, W. Yan and J. Zhang, *Carbon Energy*, 2023, **5**, e249.
51 Q. Deng, X. Dong, P. K. Shen and J. Zhu, *Adv. Sci.*, 2023, **10**, 2207470.
52 X. Dong, X. Liu, P. K. Shen and J. Zhu, *Adv. Funct. Mater.*, 2023, **33**, 2210987.
53 Y. Yan, Y. Yang, C. Fan, Y. Zou, Q. Deng, H. Liu, D. Brandell, R. Yang and Y. Xu, *ChemElectroChem*, 2022, **9**, e202200191.
54 X. Yang, S. Chen, W. Gong, X. Meng, J. Ma, J. Zhang, L. Zheng, H. D. Abruña and J. Geng, *Small*, 2020, **16**, 2004950.
55 X. Zhang, X. Bai, C. Wei, Z. Wang, B. Xi, S. Xiong and J. Feng, *Energy Environ. Sci.*, 2024, **17**, 7403–7415.
56 R. Wang, J. Jiao, D. Liu, Y. He, Y. Yang, D. Sun, H. Pan, F. Fang and R. Wu, *Small*, 2024, 2405148.
57 M. Zhao, H.-J. Peng, B.-Q. Li, X. Chen, J. Xie, X. Liu, Q. Zhang and J.-Q. Huang, *Angew. Chem., Int. Ed.*, 2020, **59**, 9011–9017.
58 X. Liu, J.-Q. Huang, Q. Zhang and L. Mai, *Adv. Mater.*, 2017, **29**, 1601759.
59 C. Adali and H. GÜNsel, *Synth. Met.*, 2024, **309**, 117759.
60 M. Liu, L. Che, Y. Zhou, N. B. S. Selabi and X. Tian, *Surf. Interfaces*, 2024, **53**, 105047.
61 H. Yan, D. Wang, Y. Tang, J. Cheng, Y. Lu, D. Zhang, J.-K. Kim and Y. Luo, *Appl. Surf. Sci.*, 2024, **677**, 161045.
62 Z. Qiao, Y. Zhang, Z. Meng, Q. Xie, L. Lin, H. Zheng, B. Sa, J. Lin, L. Wang and D.-L. Peng, *Adv. Funct. Mater.*, 2021, **31**, 2100970.
63 S. Feng, Z.-H. Fu, X. Chen and Q. Zhang, *InfoMat*, 2022, **4**, e12304.
64 Z. Shen, M. Cao, Z. Zhang, J. Pu, C. Zhong, J. Li, H. Ma, F. Li, J. Zhu, F. Pan and H. Zhang, *Adv. Funct. Mater.*, 2020, **30**, 1906661.
65 H. Ci, J. Cai, H. Ma, Z. Shi, G. Cui, M. Wang, J. Jin, N. Wei, C. Lu, W. Zhao, J. Sun and Z. Liu, *ACS Nano*, 2020, **14**, 11929–11938.
66 X. Sun, D. Tian, X. Song, B. Jiang, C. Zhao, Y. Zhang, L. Yang, L. Fan, X. Yin and N. Zhang, *Nano Energy*, 2022, **95**, 106979.
67 X. Men, T. Deng, X. Li, L. Huang and J. Wang, *J. Colloid Interface Sci.*, 2025, **678**, 345–354.
68 J. Lu, Y. Chen, Y. Zhang, J. Huang, H. Jiang, D. He and H. Chen, *J. Alloys Compd.*, 2024, **1004**, 175674.
69 Y. Jiang, T. Shi, H. Wang, A. Song, Y. Fan, Z. Ma, X. Qin and G. Shao, *J. Alloys Compd.*, 2024, **1002**, 175491.
70 X. Chen, H.-J. Peng, R. Zhang, T.-Z. Hou, J.-Q. Huang, B. Li and Q. Zhang, *ACS Energy Lett.*, 2017, **2**, 795–801.
71 Z. Yuan, H.-J. Peng, T.-Z. Hou, J.-Q. Huang, C.-M. Chen, D.-W. Wang, X.-B. Cheng, F. Wei and Q. Zhang, *Nano Lett.*, 2016, **16**, 519–527.
72 Q. Zhang, Y. Wang, Z. W. Seh, Z. Fu, R. Zhang and Y. Cui, *Nano Lett.*, 2015, **15**, 3780–3786.
73 X. Li, Y. Lu, Z. Hou, W. Zhang, Y. Zhu, Y. Qian, J. Liang and Y. Qian, *ACS Appl. Mater. Interfaces*, 2016, **8**, 19550–19557.
74 X. Lu, Q. Zhang, J. Wang, S. Chen, J. Ge, Z. Liu, L. Wang, H. Ding, D. Gong, H. Yang, X. Yu, J. Zhu and B. Lu, *Chem. Eng. J.*, 2019, **358**, 955–961.
75 N. K. Thangavel, D. Gopalakrishnan and L. M. R. Arava, *J. Phys. Chem. C*, 2017, **121**, 12718–12725.
76 H. Zhao, J. Wu, T. Chen, P. Yan, W. Yao, X. Ma, Y. Sun, W. Wang and M. Shi, *J. Energy Chem.*, 2024, **101**, 113903.
77 F. Liang, Q. Deng, S. Ning, H. He, N. Wang, Y. Zhu and J. Zhu, *Adv. Sci.*, 2024, **11**, 2403391.
78 W. Hua, H. Li, C. Pei, J. Xia, Y. Sun, C. Zhang, W. Lv, Y. Tao, Y. Jiao, B. Zhang, S.-Z. Qiao, Y. Wan and Q.-H. Yang, *Adv. Mater.*, 2021, **33**, 2101006.

79 G. Zhao, C.-W. Kao, Z. Gu, S. Zhou, L.-Y. Chang, T. Yan, C. Cheng, C. Yuan, H. Li, T.-S. Chan and L. Zhang, *ACS Appl. Mater. Interfaces*, 2022, **14**, 49680–49688.
80 M. Sun, Z. Wang, X. Li, H. Li, H. Jia, X. Xue, M. Jin, J. Li, Y. Xie and M. Feng, *J. Mater. Chem. A*, 2020, **8**, 11818–11823.
81 M. Wang, Z. Sun, H. Ci, Z. Shi, L. Shen, C. Wei, Y. Ding, X. Yang and J. Sun, *Angew. Chem., Int. Ed.*, 2021, **60**, 24558–24565.
82 X.-Y. Li, S. Feng, M. Zhao, C.-X. Zhao, X. Chen, B.-Q. Li, J.-Q. Huang and Q. Zhang, *Angew. Chem., Int. Ed.*, 2022, **61**, e202114671.
83 Q. Yu, Y. Lu, R. Luo, X. Liu, K. Huo, J.-K. Kim, J. He and Y. Luo, *Adv. Funct. Mater.*, 2018, **28**, 1804520.
84 P. Zeng, H. Zou, C. Cheng, L. Wang, C. Yuan, G. Liu, J. Mao, T.-S. Chan, Q. Wang and L. Zhang, *Adv. Funct. Mater.*, 2023, **33**, 2214770.
85 F. Wang, T. Wang, Z. Shi, S. Cui, N. Wang, G. Kang, G. Su, W. Liu and Y. Jin, *ACS Appl. Mater. Interfaces*, 2024, **16**, 55229–55239.
86 Z. Lian, L. Ma, H. Wu, H. Xiao, Y. Yang, J. Zhang, J. Zi, X. Chen, W. Wang and H. Li, *Appl. Catal., B*, 2025, **361**, 124661.
87 X. Wu, W. Xie, M. Zhao, D. Cai, M. Yang, R. Xie, C. Zhang, Q. Chen and H. Zhan, *Small*, 2024, **20**, 2406234.
88 G. Deng, W. Xi, J. Zhang, Y. Zhang, R. Wang, Y. Gong, B. He, H. Wang and J. Jin, *J. Mater. Chem. A*, 2024, **12**, 29092–29102.
89 H. Wei, Y. Gong, C. Gao, Z. Chen, Z. Zhou, H. Lv, Y. Zhao, M. Bao, K. Yu, X. Guo and Y. Wang, *Small*, 2024, **20**, 2404870.
90 P. Xia, X. Peng, L. Yuan, S. Li, S. Jing, S. Lu, Y. Zhang and H. Fan, *J. Colloid Interface Sci.*, 2025, **678**, 619–629.
91 B. Li, P. Wang, J. Yuan, N. Song, J. Feng, S. Xiong and B. Xi, *Angew. Chem., Int. Ed.*, 2024, **63**, e202408906.
92 L. Peng, M. Qu, R. Sun, W. Yang, Z. Wang, W. Sun and Y. Bai, *J. Mater. Chem. A*, 2023, **11**, 3504–3513.
93 Y.-G. Cho, C. Hwang, D. S. Cheong, Y.-S. Kim and H.-K. Song, *Adv. Mater.*, 2019, **31**, 1804909.
94 Y. Yuan, D. Zheng, Z. Fang, H. Lu, X. Gou, H. Liu and M. Liu, *Ionics*, 2019, **25**, 17–24.
95 W.-w Shao, T.-k Gao, M.-q Hu, Y.-t Ni, X.-n Fei, M.-q Liu, Z. Wang, L.-p Zhou and M.-x Jing, *J. Appl. Polym. Sci.*, 2024, **141**, e56147.
96 D. Shao, X. Wang, X. Li, K. Luo, L. Yang, L. Liu and H. Liu, *J. Solid State Electrochem.*, 2019, **23**, 2785–2792.
97 W. Chen, H. Jin, S. Xie, H. Xie, J. Zhu, H. Ji and L.-J. Wan, *J. Energy Chem.*, 2021, **54**, 16–22.
98 Z. Cui, C. Zu, W. Zhou, A. Manthiram and J. B. Goodenough, *Adv. Mater.*, 2016, **28**, 6926–6931.
99 H. Li, C. Chen, Y. Yan, T. Yan, C. Cheng, D. Sun and L. Zhang, *Adv. Mater.*, 2021, **33**, 2105067.
100 P. Li, L. Ma, T. Wu, H. Ye, J. Zhou, F. Zhao, N. Han, Y. Wang, Y. Wu, Y. Li and J. Lu, *Adv. Energy Mater.*, 2018, **8**, 1800624.
101 Z. Li, C. Zhou, J. Hua, X. Hong, C. Sun, H.-W. Li, X. Xu and L. Mai, *Adv. Mater.*, 2020, **32**, 1907444.
102 L. Liu, Z. Song, Z. Qi, L. Yang, X. Wang, Z. Hu and Q. Wu, *Chem. Commun.*, 2024, **60**, 10910–10913.
103 L. Sun, Y. Liu, J. Xie, L. Fan, J. Wu, R. Jiang and Z. Jin, *Chem. Eng. J.*, 2023, **451**, 138370.
104 G. Zhou, H. Tian, Y. Jin, X. Tao, B. Liu, R. Zhang, Z. W. Seh, D. Zhuo, Y. Liu, J. Sun, J. Zhao, C. Zu, D. S. Wu, Q. Zhang and Y. Cui, *Proc. Natl. Acad. Sci. U. S. A.*, 2017, **114**, 840–845.